

## **Comparison of SPECT Cerebral Images Examination Methods Based on Luminance Level and Morphological Spectra Evaluation**

**MAŁGORZATA PRZYTUŁSKA<sup>1,\*</sup>, JULIUSZ L. KULIKOWSKI<sup>1</sup>,  
ADAM BAJERA<sup>2</sup>, LESZEK KRÓLICKI<sup>2</sup>**

<sup>1</sup> *Institute of Biocybernetics and Biomedical Engineering, Polish Academy of Sciences, Warsaw, Poland*

<sup>2</sup> *Medical University of Warsaw, Department of Nuclear Medicine, Warsaw, Poland*

It is presented a method of SPECT (single-photon emission tomography) cerebral images examination based on morphological spectra. The advantages of the SPECT imaging in early diagnosing of encephalic diseases are emphasized. The detected radiation levels in the SPECT imaging are visualized by luminance levels which give insight into the lesions of cerebral tissue. It is shown that a rough, on luminance level based, examination of the SPECT images can be improved if more sophisticated analytical methods are used. Basic notions and properties of morphological spectra and their applicability as tools for biomedical image analysis are shortly reminded. A simple formula for reversing transformation reconstructing of original image on the basis of a given morphological spectrum is presented. Results of experiments consisting in comparison of the morphological spectra calculated for selected pairs of testing windows in the SPECT cerebral images are shown. It has been shown that the morphological spectra can better suit to an effective comparison of views of the cerebral regions located symmetrically with respect to the brain axis separating the left and right cerebral hemispheres than the averaged luminance level.

**K e y w o r d s:** computer-assisted image processing, brain imaging, SPECT imaging, morphological spectra

### **1. Introduction**

Modern medical imaging methods are aimed at low-invasive inspection into anatomy, morphology and/or functions of inner human organs. So, they became one of the

---

\* Correspondence to: Małgorzata Przytułska, Institute of Biocybernetics and Biomedical Engineering, Polish Academy of Sciences, ul. Ks. Trojdena 4, 02-109 Warsaw, Poland, e-mail: mprzytułska@ibib.waw.pl  
*Received 10 April 2008; Accepted 23 September 2008*

most powerful tools of medical diagnosis, very important in early detection of the most dangerous and frequently occurring diseases. Physicians have at their disposal a large variety of medical imaging modalities, like: X-ray imaging, ultrasonography (USG), computer tomography (CT), single-photon emission tomography (SPECT), positron-emission tomography (PET), nuclear magnetic resonance (NMR), thermography (ThG), etc. [1, 2]. In each of the above-mentioned cases medical applicability, imaging quality, costs, and invasiveness are the main features taken into consideration in the medical imaging modality assessment.

To each medical diagnostic problem the most preferable imaging modalities can be assigned. In particular, the demands for preliminary and rough on one hand, and deeper and more accurate diagnostic methods on the other hand, may lead to different preferences in choosing the right imaging modalities. In emergent medical cases (e.g. cardiac infarct, cerebral stroke, arterial embolism, etc.) high diagnostic sensitivity and short time of decision-making may be critical in patients' life saving. Screening medical examinations aimed at early detection of dangerous in social sense and scale diseases are usually based on high sensitivity, low cost diagnostic procedures. High diagnostic specificity and high accuracy localization of stricken by a disease inner organ's area become highly important in planning advanced therapeutic procedures (e.g. surgical intervention, radiological treatment, etc.). That is why, despite the development of the modern medical imaging modalities (PET, NMR), some older ones are still used and improved [3]. The SPECT imaging based on the principle of reconstruction of  $\gamma$ -type radiation intensity distribution map caused by a radionuclide introduced to the examined organ belong to such methods. Modern  $\gamma$ -cameras (containing rotating rings of  $\gamma$ -detectors) used to the SPECT images acquisition reduce the image acquisition time to several minutes and deliver radiological images of  $128 \times 128$  pixels standard. This may seem to be rather poor in comparison to other modalities (X-ray, CT, USG), however, a high tissue specificity (if adequate nuclides are used) makes the SPECT imaging competitive to the other ones in soft organs (brain, thyroid, liver, heart, kidneys, etc.) examinations. The simplest way to various tissues discrimination in the SPECT imaging technique is based on a comparison of radiation intensity registered in selected image areas [1, 2]. A rough diagnostic interpretation of so-obtained data is possible due to a visualization of a map of radiation intensity distribution in a given observation area. However, a deeper diagnosis based on numerical parameters needs using a computer-assistant image processing technique. In such case the radiation intensity map should be imposed on the anatomical scheme of an examined organ, regions of interest should be selected, geometrical and/or morphological parameters should be evaluated and the vectors of parameters should be subjected to a final diagnostic interpretation. In particular, they quantitatively characterize the anatomically localized regions of abnormal penetration levels into the observed organ of a nuclide marker. From a formal point of view the registered radiation intensity is a 2D image changing slowly in time. This means that useful diagnostic information is delivered by its relative rather than by absolute local values. Moreover, spatial resolution of

the images determines their ability to visualize fine morphological structures existing in the examined objects. Spatial averaging of local radiation intensity values causes thus a loss of information useful to discrimination of tissues of different micro-morphological structure. Saving of this information is possible, if micro-morphological structures, visible as specific textures covering the selected parts of images, together with locally averaged radiation intensities in radiological image examination are taken into consideration. General methods of texture analysis are widely described in the literature; for this purpose various concepts based on spectral or statistical approaches were proposed [4–8]. However, the problem of choosing the most suitable method of the cerebral images analysis is still open. The problem consists both in a detection of differences of textures and an accurate segmentation of the areas where the differences are medically significant. That is why a series of works aimed at proving and comparing several methods has been undertaken within a collaboration of the authors representing both, engineering and medical approach to the problem. In [9] a simple approach based on the mean values and standard deviations of local luminance levels has been presented. In [10] simple statistical approach has been compared to the entropy and fractal dimension based methods. In this paper a concept of using the morphological spectra to analysis of radiological SPECT images is presented.

The idea of the morphological spectra as tools for texture analysis was originally proposed in [11, 12]. The morphological spectra seem to have several interesting properties as the tools of texture analysis: they are simple to be calculated, they can be used to image enhancement and due to their hierarchical structure they make possible analysis of the textures on different levels of morphological structures detailing. However, in this paper our attention is focused on the aspect of differences between the textures detection.

The organization of this paper is as follows. In Sec. 2 of the paper basic notions and properties of the morphological spectra are shortly reminded. Experiments performed on the SPECT human brain images analyzed with 4th level morphological spectra are described in Sec. 3. Sec. 4 contains conclusions and some suggestions concerning further works.

## 2. Selected Properties of the Morphological Spectra

Morphological spectra are defined for 2D monochromatic images represented by bit-maps of  $2^m \times 2^n$  size, where  $m$  and  $n$  are fixed natural numbers. Other sizes of the bit-maps are admissible, however, in such case the bitmap should be extended (by adding 0-values) to the nearest standard size. The morphological spectra form a hierarchical, multi-level structure. The highest level  $k^*$  of the morphological spectra is given by  $k^* = \min(m, n)$ . The spectral components of  $k$ -th level,  $0 \leq k \leq k^*$ , are calculated on basic windows having the form of  $2^k \times 2^k$  squares. The components of 0<sup>th</sup> level spectrum are by definition identical to the pixel values of the original image. For

calculation of the spectral components the image is partitioned into  $2^{m-k} \times 2^{n-k}$  adjacent basic windows and the values of a given spectral component for each basic window are calculated independently. Thus, the spectral component of the total image takes the form of a  $2^{m-k} \times 2^{n-k}$  real matrix. The  $k$ -th level morphological spectrum consists of  $2^{2k}$  components. The components are labeled and can be lexicographically ordered by  $k$ -element strings of symbols  $\Sigma, V, H, X$ . Therefore, the 1<sup>st</sup> level morphological spectrum consists of the components  $\Sigma, V, H$  and  $X$  only. The 2<sup>nd</sup> level morphological spectrum consists of 16 components:  $\Sigma\Sigma, \Sigma V, \Sigma H, \Sigma X, V\Sigma, VV, VH, VX, H\Sigma, HV, HH, HX, X\Sigma, XV, XH$  and  $XX$ , etc.<sup>a</sup>

The components of the morphological spectra can be represented by a tree with nodes assigned to the components and edges corresponding to the relationships of direct hierarchical connections between the components of two consecutive spectrum levels. The root of the tree is assigned to the 0<sup>th</sup> level component (the initial image bit-map). For calculation of the spectral components special binary matrices called *spectral masks* are used. For the 1<sup>st</sup> level morphological spectra the masks have the following form (for the sake of simplicity the masks are denoted by the same symbols as the corresponding spectral components excepting that they are printed in bolds):

$$\Sigma = \begin{bmatrix} 1 & 1 \\ 1 & 1 \end{bmatrix}, \quad V = \begin{bmatrix} -1 & 1 \\ -1 & 1 \end{bmatrix}, \quad H = \begin{bmatrix} -1 & -1 \\ 1 & 1 \end{bmatrix}, \quad X = \begin{bmatrix} -1 & 1 \\ 1 & -1 \end{bmatrix}. \quad (1)$$

Then calculation of the spectral components is based on a *direct product* of matrices defined as follows. If there are given two matrices of equal sizes:  $A = [a_{p,q}]$  and  $B = [b_{p,q}]$  then their direct product is defined as a matrix  $C = A \bullet B = [a_{p,q} \cdot b_{p,q}]$ , saving the size of its components. Therefore, if  $\Xi = [\xi_{p,q}]$  is a  $2 \times 2$ -size basic window of a bit-map ( $\xi_{p,q}$  denoting the corresponding pixel value), the following direct products of the matrices can be calculated:

$$\Sigma \bullet \Xi = \begin{bmatrix} \xi_{1,1} & \xi_{1,2} \\ \xi_{2,1} & \xi_{2,2} \end{bmatrix}, \quad V \bullet \Xi = \begin{bmatrix} -\xi_{1,1} & \xi_{1,2} \\ -\xi_{2,1} & \xi_{2,2} \end{bmatrix}, \quad H \bullet \Xi = \begin{bmatrix} -\xi_{1,1} & -\xi_{1,2} \\ \xi_{2,1} & \xi_{2,2} \end{bmatrix}, \quad X \bullet \Xi = \begin{bmatrix} -\xi_{1,1} & \xi_{1,2} \\ \xi_{2,1} & -\xi_{2,2} \end{bmatrix}. \quad (2)$$

Finally, the spectral components are calculated as sums of the elements of the corresponding matrices:

$$\left. \begin{aligned} v_{\Sigma} &= \xi_{1,1} + \xi_{1,2} + \xi_{2,1} + \xi_{2,2}, & v_V &= -\xi_{1,1} + \xi_{1,2} - \xi_{2,1} + \xi_{2,2}, \\ v_H &= -\xi_{1,1} - \xi_{1,2} + \xi_{2,1} + \xi_{2,2}, & v_X &= -\xi_{1,1} + \xi_{1,2} + \xi_{2,1} - \xi_{2,2} \end{aligned} \right\}. \quad (3)$$

The spectral components of higher level can be calculated in similar way; however, the  $k$ -th level masks take the form of  $2^{2k} \times 2^{2k}$  matrices and the direct products are calculated for  $2^{2k} \times 2^{2k}$ -size basic windows. The 2<sup>nd</sup> and 3<sup>rd</sup>-level masks are available in [8].

<sup>a</sup> Spectral components can also be defined using systems of orthogonal Walsh functions.

The morphological spectra can also be calculated by using an unified model. For this purpose the masks of a given level are presented in the form of *spectral matrices* of  $2^{4k} \times 2^{4k}$  size of which rows correspond to lexicographically ordered spectral components and columns are assigned to lexicographically ordered pixels in the basic windows. For example, the 1<sup>st</sup> level masks given by (1) will be represented by the spectral matrix:

$$\mathbf{M}^{(1)} = \begin{bmatrix} 1 & 1 & 1 & 1 \\ -1 & 1 & -1 & 1 \\ -1 & -1 & 1 & 1 \\ -1 & 1 & 1 & -1 \end{bmatrix}. \quad (4)$$

Spectral matrices of any level are orthogonal matrices, i.e. such that

$$\mathbf{M}^{(k)} \cdot (\mathbf{M}^{(k)})^{tr} = (\mathbf{M}^{(k)})^{tr} \cdot \mathbf{M}^{(k)} = 2^{2k} \cdot \mathbf{I} \quad (5)$$

where <sup>tr</sup> denotes matrix transposition and  $\mathbf{I}$  is an unity matrix of  $2^{4k} \times 2^{4k}$  size. If the basic window  $\mathcal{E}$  is expanded into a vector:

$$\mathbf{U}^{(k)} = [\xi_{1,1}, \xi_{1,2}, \dots, \xi_{1,n}, \xi_{2,1}, \dots, \xi_{2,n}, \dots, \xi_{m,1}, \dots, \xi_{m,n}] \quad (6)$$

then the morphological spectrum can be calculated as:

$$(\mathbf{V}^{(k)})^{tr} = \mathbf{M}^{(k)} \cdot (\mathbf{U}^{(k)})^{tr}. \quad (7)$$

Multiplying both sides of (7) on the left by  $(\mathbf{M}^{(k)})^{tr}$  and taking (5) into account we obtain:

$$(\mathbf{M}^{(k)})^{tr} \cdot (\mathbf{V}^{(k)})^{tr} = 2^{2k} \cdot (\mathbf{U}^{(k)})^{tr} \quad (8)$$

and finally:

$$\mathbf{U}^{(k)} = 2^{-2k} \cdot \mathbf{V}^{(k)} \cdot \mathbf{M}^{(k)}. \quad (9)$$

Therefore, this is a very simple formula for the bit-map  $\mathbf{U}^{(k)}$  reconstruction when its morphological spectrum  $\mathbf{V}^{(k)}$  is given.

### 3. Using the Morphological Spectra to Analysis of the SPECT Brain Images

In rough early diagnosis of certain types of encephalopathy a comparison of the views of respective areas in the left and right cerebral hemisphere in radionuclide

images plays an important role. The differences may indicate the regions of encephalitis, encephalomalacia, encephalorrhagia, cerebral ischaemia, epileptic foci, etc. High diagnostic sensitivity of difference detection is a crucial point in this type of diagnostic procedure. A comparison of luminance levels in the corresponding brain image areas, chosen symmetrically with respect to the cerebral axis, is the simplest method of cerebral pathological changes detection. However, this approach neglects the morphological details of cerebral structures under observation. It may happen that they contain useful diagnostic information despite the fact that no noticeable difference between the mean luminance levels in the regions under observation occurs. In such case the additional information may be supplied by a comparison of the morphological spectra of the observed regions. For this purpose, analyzed images should be divided into square windows localized symmetrically with respect to the main cerebral axis. The size of the windows should be chosen so as to satisfy the conditions of being used as the basic windows in the morphological spectra calculation. Then, the morphological spectra of symmetrically chosen pairs of windows should be calculated and compared.

The differences between the pairs of the morphological spectra in several ways can be evaluated. In the simplest case the spectra can be considered as real vectors and the distance measures (absolute, Euclidean, Tshebyshevian, etc.) between the vectors can be calculated. An alternative, more advanced approach may consist in emphasizing the role of selected vector components according to the morphological specificity of the examined brain regions. In this paper the first approach is considered only.

The aim of investigation consisted in proving the general usefulness of the morphological spectra to detect differences between selected areas in brain images caused by their different ability to absorb the nuclide markers. The experiments had to show, whether and how much an intuitive similarity assessment of selected pairs of fragments of cerebral images can be improved by using a quantitative comparison of the morphological spectra of the corresponding fragments. For this purpose 10 SPECT images of human brains (delivered from the Department of Nuclear Medicine of the Medical Academy in Warsaw) were examined. The images were of  $128 \times 128$  pixels size, according to a typical standard of the SPECT images. Examination of the images consisted of the following steps:

1. Each image was partitioned into 64 square testing windows of  $16 \times 16$  pixels size which have been labeled by their row (from 1 to 8) and column (from A to H) indexes.

2. From each image 10 pairs of the testing windows have been selected so that five of them corresponded to the regions classified as "similar" and five other classified as "dissimilar" ones. So, there were obtained two testing sets of pairs of the "similar" and "dissimilar" testing windows. The so obtained testing sets represented a human intuitive understanding of "similarity" and of "dissimilarity" of image regions visualizing different types or states of cerebral tissues.

3. For each testing window the following (16 of 256 possible) 4<sup>th</sup> level morphological spectrum components:

$$\Sigma\Sigma\Sigma\Sigma, \Sigma\Sigma\Sigma V, \Sigma\Sigma\Sigma H, \Sigma\Sigma\Sigma X, \Sigma\Sigma V\Sigma, \Sigma\Sigma VV, \Sigma\Sigma\Sigma VH, \Sigma\Sigma VX, \Sigma\Sigma H\Sigma, \Sigma\Sigma HV, \Sigma\Sigma HH, \Sigma\Sigma HX, \Sigma\Sigma X\Sigma, \Sigma\Sigma XV, \Sigma\Sigma XH, \Sigma\Sigma XX$$

were calculated. Each spectral component denoted as  $\Sigma\Sigma PQ$ , where  $P, Q \in \{\Sigma, V, H, X\}$ , represents in fact a sum of 2<sup>nd</sup> level  $PQ$  spectral component values taken from adjacent square sub-windows of  $4 \times 4$  size, as illustrated in Fig. 1. This has been done in order to reduce 4 times the variance of the  $PQ$  component evaluation caused by random factors.

4. The 4<sup>th</sup> level spectral components were considered as 16-component vectors and for the selected pairs of testing windows the Euclidean distances of vectors were calculated. Let  $\mathbf{u}_{\alpha\beta}$ ,  $\alpha \in \{1, 2, \dots, 8\}$ ,  $\beta \in \{A, B, \dots, H\}$  denote a 16-component spectral vector of a testing window addressed by  $(\alpha, \beta)$ . Then the distances of the spectral vectors are described by the formula:

$$d(\mathbf{u}_{\alpha\beta}, \mathbf{u}_{\varepsilon\eta}) = \sqrt{\sum_{\kappa=1}^{16} (|u_{\alpha\beta}^{(\kappa)}| - |u_{\varepsilon\eta}^{(\kappa)}|)^2} \tag{10}$$

where  $u_{\alpha\beta}^{(\kappa)}$ ,  $u_{\varepsilon\eta}^{(\kappa)}$  denote, correspondingly, the  $\kappa$ -th components of the spectral vectors  $\mathbf{u}_{\alpha\beta}$ ,  $\mathbf{u}_{\varepsilon\eta}$ . The distance has been calculated for absolute values of the spectral components in order to avoid a dependence of the result on parallel shifts of the testing windows which may cause random changes of the signs of the components [12].

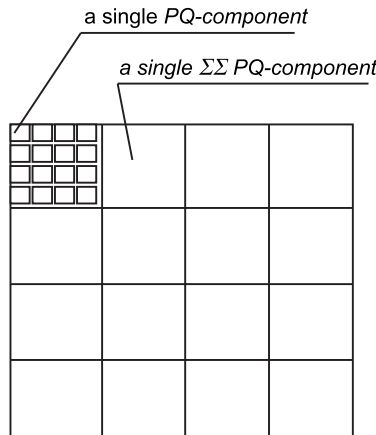


Fig. 1. Structure of a testing window

Then the calculated distances have been non-increasingly ordered for a visualization of their range of variation. Taking into account that a maximal distance of the spectral vectors corresponds to the minimal similarity of the testing windows and *vice versa*, the ordered sequence of distances also illustrates the variations of similarities. The results of calculations performed on a selected image are shown

below. In Figure 2 the position of 10 selected pairs of the testing windows in the given SPECT image is indicated by arrows, while Fig. 3 presents the corresponding sequence of ordered distances. It is interesting to observe that the largest distances of the spectral vectors do not obviously correspond to the pairs of the testing windows which seem to be rather “similar” (e.g., see the pair #3 (4F-5C)). On the other hand, some pairs of the testing windows, e.g. #9 (3B-6D) or #10 (3B-5C) seem to be “dis-similar” while their spectral distances are relatively small. In order to investigate this paradox it was defined a *relative variations range* (*RVR*) of luminance, symbolically denoted by  $\lambda$  and given by the formula:

$$\lambda = \frac{|\sum\sum\sum\sum\alpha\beta - \sum\sum\sum\sum\varepsilon\eta|}{\max(\sum\sum\sum\sum\alpha\beta, \sum\sum\sum\sum\varepsilon\eta)} \cdot 100\% . \quad (12)$$

The *RVR* of luminance takes value 100% if exactly one of the components  $\sum\sum\sum\sum\alpha\beta$  or  $\sum\sum\sum\sum\varepsilon\eta$  takes value 0 and it takes value 0% if both the components are equal. The values of spectral distances and of the *RVR* of luminance in the above-presented example are given in Table 1.

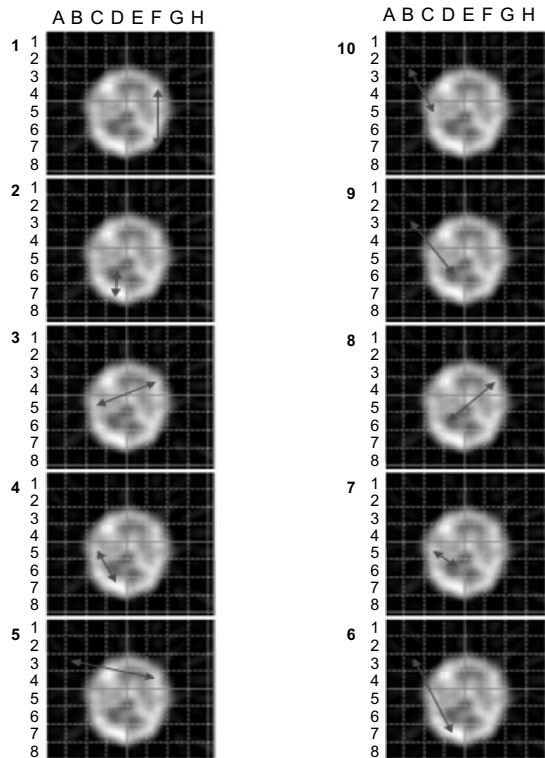


**Fig. 2.** A cerebral SPECT image with 10 pairs of the testing windows selected for comparison of their morphological spectra



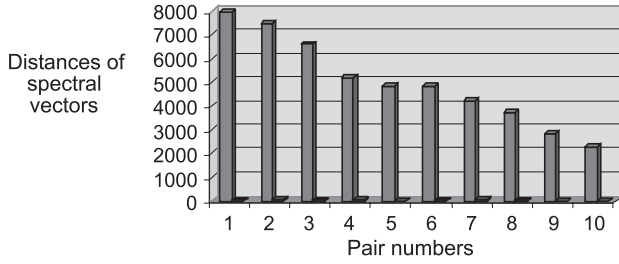


**Fig. 3.** Non-increasingly ordered sequence of distances (in pixels) of the pairs of spectral vectors corresponding to the testing windows indicated in Fig. 2

**Table 1.** Distances (in pixels) of the pairs of spectral vectors

No of the pair	Pair of testing windows	Distance of spectral vectors	$\lambda$ (%)
1	4F-7D	7990,372	19.89
2	6D-7D	7493,312	12.37
3	4F-5C	6631,004	9.697
4	5C-7D	5173,26	11.29
5	3B-4F	4825,785	97.99
6	3B-7D	4818,821	98.39
7	5C-6D	4187,57	1.212
8	4F-6D	3716,497	8.589
9	3B-6D	2809,894	98.16
10	3B-5C	2318,017	98.18

It is interesting to see that the similarity of pairs of the testing windows evaluated on the basis of distance measures of the spectral vectors does not always coincide with those intuitively assessed by visual comparison of the testing windows. The pairs #3: 4F – 5C ( $d = 6631.004$ ) and #4: 5C – 7D ( $d = 5173.26$ ) belonging to the left part of the graph represent here “dissimilar” pairs of spectral vectors. However, the *RVRs* of luminance are: for 4F – 5C  $\lambda = 5.85\%$ , for 5C – 7D  $\lambda = 6.84\%$ ; they are thus rather low and this is why the corresponding pairs of the testing windows intuitively seem to be “similar”. This suggests that the real differences between the testing windows are here represented by other, not easily visible spectral components.

On the other hand, looking at the pair #9: 3B – 6D one assess it as “dissimilar”, the *RVR* of luminance being  $\lambda = 96.39\%$ . However, a relatively small spectral distance ( $d = 2809.894$ ) leads to a classification of this pair as “similar”.

Calculations of similar type have been performed for other SPECT images. In each image distances of the spectral vectors for selected 10 pairs of the testing windows were calculated and the minimal and maximal distances were found. Then the *RVRs* of spectral distances according to the formula:

$$\mu = \frac{d_{\max} - d_{\min}}{d_{\max}} \cdot 100\% \quad (13)$$

have been calculated. The higher is  $\mu$ , the larger is the possibility of the pairs of the testing windows discrimination on the basis of their spectral distances. In Table 2 the results are presented together with the corresponding *RVRs* of luminance level.

**Table 2.** Relative variations ranges of spectral distances (in pixels) and luminance level evaluated in the selected images

No of image	$d_{\max}$	$d_{\min}$	$\mu$ %	$\lambda_{\max}$	$\lambda_{\min}$	$\lambda$ %
#1	5014.93	2197.54	<b>56.18</b>	186	3	<b>98.38</b>
#2	2913.88	151.77	<b>94.79</b>	180	2	<b>98.89</b>
#3	4491.36	740.73	<b>83.51</b>	161	1	<b>99.38</b>
#4	3389.09	485.14	<b>85.69</b>	212	0	<b>100.00</b>
#5	1920.62	363.57	<b>81.07</b>	146	0	<b>100.00</b>
#6	3129.45	304.20	<b>90.28</b>	210	3	<b>98.57</b>
#7	3632.05	435.72	<b>87.98</b>	213	4	<b>98.12</b>
#8	5351.49	106.51	<b>98.01</b>	185	2	<b>98.92</b>

At a first glance it might seem that the *RVRs* of luminance ( $\lambda$ ) better suit to discrimination of the differences between the testing windows than those of spectral distances ( $\mu$ ). However, high values of  $\lambda$  reaching 100% are caused by the fact that minimal luminance levels in certain images (#4 and #5) are equal 0, while the norm of the spectral vectors may be equal 0 only in the case of a totally black image. The results suggest that discriminative power of the different spectral components may be different, the luminance level (represented by the  $\Sigma\Sigma\Sigma\Sigma$  component) being one of them. In order to prove it for the selected images the *RVRs* of all the spectral components were calculated. Table 3 presents the results obtained for one selected image (#2).

**Table 3.** Relative variations range of the spectral components of a selected image (#2)

Comp.	$\Sigma\Sigma\Sigma\Sigma$	$\Sigma\Sigma\Sigma V$	$\Sigma\Sigma\Sigma H$	$\Sigma\Sigma\Sigma X$	$\Sigma\Sigma V\Sigma$	$\Sigma\Sigma V V$	$\Sigma\Sigma V H$	$\Sigma\Sigma V X$
Min.	2	205	52	35	97	3	4	7
Max.	180	1391	2586	734	641	316	366	88
$\lambda$ (%)	<b>98.89</b>	85.26	97.99	95.23	84.87	<b>99.05</b>	<b>98.91</b>	92.05

Comp.	$\Sigma\Sigma H\Sigma$	$\Sigma\Sigma H V$	$\Sigma\Sigma H H$	$\Sigma\Sigma H X$	$\Sigma\Sigma X\Sigma$	$\Sigma\Sigma X V$	$\Sigma\Sigma X H$	$\Sigma\Sigma X X$
Min.	20	20	4	1	11	0	7	1
Max.	1250	366	642	82	208	43	48	43
$\lambda$ (%)	98.40	94.54	<b>99.38</b>	98.78	94.71	<b>100.0</b>	85.42	97.67

It can be observed that four spectral components:  $\Sigma\Sigma VV$ ,  $\Sigma\Sigma VH$ ,  $\Sigma\Sigma HH$  and  $\Sigma\Sigma XV$  have higher *RVRs* (signed in bold) than this based on luminance level ( $\Sigma\Sigma\Sigma\Sigma$ ). A similar situation was observed in other images. This means that not only other (besides the luminance level) spectral components can discriminate the differences between the testing windows but also they are sensitive to their specific morphological structures. In Table 4 there are presented the spectral components that in the selected images have been observed as having the highest *RVRs*.

**Table 4.** Spectral components having the highest *RVRs* ( $\lambda$ ) in the selected analysed images

Nr of image	1 <sup>st</sup> comp $\lambda$ (%)	2 <sup>nd</sup> comp $\lambda$ (%)	3 <sup>rd</sup> comp $\lambda$ (%)	4 <sup>th</sup> comp $\lambda$ (%)	5 <sup>th</sup> comp $\lambda$ (%)	6 <sup>th</sup> comp $\lambda$ (%)
#1	$\Sigma\Sigma\Sigma X$ 99.57	$\Sigma\Sigma\Sigma V$ 99.25	$\Sigma\Sigma HV$ 98.43	$\Sigma\Sigma XV$ 98.61	$\Sigma\Sigma\Sigma\Sigma$ 98.39	$\Sigma\Sigma V\Sigma$ 97.68
#2	$\Sigma\Sigma XV$ 100.0	$\Sigma\Sigma HH$ 99.38	$\Sigma\Sigma VV$ 99.05	$\Sigma\Sigma VH$ 98.91	$\Sigma\Sigma HX$ 98.78	$\Sigma\Sigma H\Sigma$ 98.40
#3	$\Sigma\Sigma\Sigma\Sigma$ 99.38	$\Sigma\Sigma\Sigma H$ 98.57	$\Sigma\Sigma XV$ 98.46	$\Sigma\Sigma H\Sigma$ 98.04	$\Sigma\Sigma VX$ 97.96	$\Sigma\Sigma XX$ 97.62
#5	$\Sigma\Sigma\Sigma\Sigma$ 100.0	$\Sigma\Sigma VH$ 99.15	$\Sigma\Sigma\Sigma V$ 98.19	$\Sigma\Sigma XV$ 97.67	$\Sigma\Sigma XH$ 97.33	$\Sigma\Sigma V\Sigma$ 96.53
#6	$\Sigma\Sigma\Sigma V$ 99.73	$\Sigma\Sigma\Sigma H$ 99.49	$\Sigma\Sigma X\Sigma$ 99.19	$\Sigma\Sigma\Sigma\Sigma$ 98.57	$\Sigma\Sigma\Sigma X$ 98.40	$\Sigma\Sigma H\Sigma$ 98.42

The spectral components that occur in this table have the following frequencies:  $\Sigma\Sigma\Sigma\Sigma$  and  $\Sigma\Sigma XV$  – 4 times;  $\Sigma\Sigma\Sigma V$ ,  $\Sigma\Sigma\Sigma H$  and  $\Sigma\Sigma H\Sigma$  – 3 times,  $\Sigma\Sigma V\Sigma$  and  $\Sigma\Sigma VH$  – 2 times,  $\Sigma\Sigma\Sigma X$ ,  $\Sigma\Sigma VV$ ,  $\Sigma\Sigma VX$ ,  $\Sigma\Sigma HV$ ,  $\Sigma\Sigma HH$ ,  $\Sigma\Sigma HX$ ,  $\Sigma\Sigma X\Sigma$ ,  $\Sigma\Sigma XH$  and  $\Sigma\Sigma XX$  – 1 time. The most frequently occurring components, as the most highly discriminating the differences between the testing windows can be recommended to be used to the analysis of the cerebral SPECT images.

In order to compare the discriminating power of luminance and other spectral components from several images there were selected 10 pairs of the testing windows symmetrically located with respect to the central vertical axis of the image. Such pairs are those that should be analyzed in the cerebral SPECT images. For the selected pairs there were taken into consideration the above-mentioned most recommended spectral components:  $\Sigma\Sigma\Sigma\Sigma$ ,  $\Sigma\Sigma XV$ ,  $\Sigma\Sigma\Sigma V$ ,  $\Sigma\Sigma\Sigma H$  and  $\Sigma\Sigma H\Sigma$ . Then the *relative differences* of component values for the given pairs of testing windows were calculated according to the formula:

$$\eta = \frac{|u' - u''|}{\max(u', u'')} \cdot 100\% \tag{14}$$

where  $u'$ ,  $u''$  denote the measured values of a given spectral component in the pair of the testing windows under consideration. Thus the higher  $\eta$ , the more sensible is

the given spectral component to the difference between the contents of the compared testing windows. The results are presented in Table 5.

**Table 5.** Relative differences of the selected spectral components applied to evaluate the pairs of the symmetrically located testing windows

Image	Pair of testing windows	Spectral distance (in pixels)	$\Sigma\Sigma\Sigma\Sigma$ $\eta$ %	$\Sigma\Sigma X V$ $\eta$ %	$\Sigma\Sigma\Sigma V$ $\eta$ %	$\Sigma\Sigma\Sigma H$ $\eta$ %	$\Sigma\Sigma\Sigma H$ $\eta$ %
#3	3D-3E	999.83	9.02	94.73	74.14	31.43	31.28
#3	4D-4E	1076.23	4.35	0.0	0.0	23.63	22.97
#3	7D-7E	1875.37	5.30	47.69	87.07	50.78	69.27
#4	3D-3E	1338.01	3.51	57.89	90.21	71.36	55.68
#5	3D-3E	1152.59	6.25	87.50	57.92	82.01	19.66
#5	7D-7E	1771.88	3.03	74.19	38.05	72.69	38.77
#6	1B-1G	304.20	40.0	83.33	98.57	77.42	59.26
#6	3D-3E	3044.03	6.06	93.55	43.78	9.28	5.81
#6	4D-4E	1310.57	2.38	50.0	40.63	19.28	21.27
#6	6C-6F	772.34	26.32	59.26	12.18	46.44	48.79

It can be observed that in most cases the relative differences of the values of the components  $\Sigma\Sigma X V$ ,  $\Sigma\Sigma\Sigma V$ ,  $\Sigma\Sigma\Sigma H$  and  $\Sigma\Sigma\Sigma H$  are higher than those of  $\Sigma\Sigma\Sigma\Sigma$ . This means that the given components better differentiate the contents of the testing windows than the average luminance level.

#### 4. Conclusions

Morphological spectra are a flexible tool for medical images examination in the cases when discrimination of tissues is a basis of diagnostic reasoning. Calculation of the morphological spectra as well as reconstruction of the original image on the basis of its morphological spectrum is described by very simple algebraic operations. The morphological spectra, in particular, can be used to analysis of the cerebral SPECT images in order to detect the differences between areas localized symmetrically with respect to the axis separating the left and right cerebral hemispheres. An advantage of the approach to cerebral image analysis based on the morphological spectra in comparison to the statistical methods presented in [5] and [6] consists in the ability of a selection of image areas (regions of interest) based not only on luminance level (i.e. on its mean value, variance, etc.) but also on the specific isotropic or anisotropic morphological texture properties. It has been shown that some 4th level morphological spectral components, defined on  $16 \times 16$  pixels testing windows, better discriminate the morphological properties of textures than the average luminance-level parameter. As such, they can better suite to detection of fine differences between the selected

regions of the left and the right cerebral hemisphere. In the forthcoming, a similar analysis of the 3rd level morphological spectra (of which components are defined on  $8 \times 8$  testing windows, and thus, they admit image analysis with better resolution power) should be performed. However, good discriminative properties of the selected morphological spectral components should not obviously correspond to the cerebral tissues properties being of the high medical importance. Therefore, the proposed method of the cerebral SPECT images analysis should be verified on a larger set of clinical data provided with independent medical diagnoses.

### Acknowledgment

This work has been realized as a research project No St/2.4/08 of the Institute of Biocybernetics and Biomedical Engineering PAS, and project No 4211/BT02/2007/33, supported by the Ministry of Science and Higher Education of Poland.

### References

1. Israel O., Goldsmith S.J. (Eds.): Hybrid SPECT/CT Imaging in Clinical Practice. Taylor & Francis, New York 2006.
2. Rumiński J., Kalicka R., Bobek-Billewicz B.: Parametric Imaging in brain investigation by MRI/PET methods, Wyd. Gdańskie, Sp.z.o.o., Gdańsk 2006, (in Polish).
3. Leemput K. Van., Vandermeulen D., Maes F., Srivastava S., D'Agostino E., Suetens P.: Model-Based Brain Tissue Classification. In: J.S. Suri, D.L. Wilson, S. Laxminarayan (Eds.): Handbook of Biomedical Image Analysis. Vol. I, Segmentation Models, Part B. Kluwer Academic/Plenum Publishers, New York 2005, 1–45.
4. Bruno A., Collorec R., Bezy-Wendling J. et al.: Texture Analysis in Medical Imaging. In: Roux C., Coatrieux J.-L. (Eds.), Contemporary Perspectives in Three-Dimensional Biomedical Imaging. IOS Press, Amsterdam 1997.
5. Haddon J.F., Boyce J.F.: Texture Segmentation and Region Classification by Orthogonal Decomposition of Cooccurrence Matrices. Proc. 11<sup>th</sup> IAPR Intern. Confer. on Pattern Recognition, Hague, IEEE Computer Society Press, Los Alamitos 1992, 692–695.
6. Ojala T., Pietikajnen M.: Unsupervised Texture Segmentation Using Feature Distributions, Texture Analysis Using Pairwise Interaction Maps. Image Analysis and Processing, 9<sup>th</sup> Intern. Confer., ICIAP'97, Proc. (A. Del Bimbo ed.), Florence 1997, I, 311–318.
7. Farag A.A., Ahmed M.N., El-Baz A., Hassan H.: Advanced Segmentation Techniques. In: J.S. Suri, D.L. Wilson, S. Laxminarayan (Eds.) Handbook of Biomedical Image Analysis. Vol. I, Segmentation Models, Part A. Kluwer Academic/Plenum Publishers, New York 2005, 479–533.
8. Yang S., Mitra S.: Statistical and Adaptive Approaches for Optimal Segmentation in Medical Images. In: Suri J.S., Wilson D.L., Laxminarayan S. (Eds.) Handbook of Biomedical Image Analysis. Vol. I, Segmentation Models, Part B. Kluwer Academic/Plenum Publishers, New York 2005, 267–314.
9. Przytułska M., Kulikowski J.L., Bajera A.: A Comparative Analysis of SPECT Images of the Left and Right Cerebral Hemispheres in Patients with Diagnosed Epileptic Symptoms. In: E. Kački (Ed.) Computers in Medical Activity, (to occur), 2008.
10. Olejarczyk E., Przytułska M., Bajera A., Królicki L.: Comparative Analysis of the SPECT Images of the Left and Right Cerebral Hemispheres in Patients with Epileptic Symptoms. Biocybernetics and Biomedical Engineering, 2008, 28 (to occur).

11. Kulikowski J.L., Przytulska M., Wierzbicka D.: Recognition of Textures Based on Analysis of Multilevel Morphological Spectra. IFMBE Proceedings, World Congress, Seoul 2006, 14, 2164–2167.
12. Kulikowski J.L., Przytulska M., Wierzbicka D.: Morphological Spectra as Tools for Texture Analysis. In: Kurzynski M. et al. (Eds.), Computer Recognition Systems 2 . Advances in Soft Computing 45, Springer, Berlin 2007.